Vibration Suppression of Two-Wheel Mobile Manipulator Using Resonance-Ratio-Control-Based Null-Space Control

Pradeep K. W. Abeygunawardhana and Toshiyuki Murakami, *Member, IEEE*

***Abstract*—A two-wheel mobile manipulator has the potential to become a multiskilled robot in the field of robotics, and it is already implemented by using inverted pendulum control. The center of gravity (COG) position is controlled to achieve the balancing of the robot. Since the vibrations of manipulator arms affect the COG positions of the inverted pendulum, balancing of the robot deteriorates. Therefore, the vibration control of manipulator arms of the two-wheel mobile manipulator is proposed in this paper. The virtual double-inverted pendulum is modeled using a "4-DOF" manipulator, and it is controlled in work space and null space. Resonance ratio control is utilized for vibration-suppression control. The resonance ratio of a system can be determined arbitrarily by the feedback of reaction torque, and reaction torque observers are implemented for each and every manipulator motor. The feedback signal for vibration suppression is introduced to the null space of the manipulator. Simulations and experiments were carried out to check the validity of the proposed method, and results prove the effectiveness of the proposed vibration controller.**

***Index Terms*—Acceleration control, null space, resonance ratio control, two-wheel mobile manipulator, vibration-suppression control.**

I. Introduction

MULTISKILLED robots are becoming popular in household use, as well as in industrial use. Recently, household multiskilled robots, which can perform most of the household chores, have been developed in Japan. A two-wheel mobile manipulator can also be considered as a multiskilled robot due to its ability to move and perform some tasks using the manipulator part. Mobile manipulation provides dual advantages of mobility and dexterity that are offered by the platform and the manipulator, respectively. The degree of freedom of the platform has added the redundancy of the system. These systems can be used effectively for a variety of tasks, such as industrial robots, service robotics, etc. Meanwhile, the inverted pendulum problem is one of the common problems in control engineering. The technology that evolved from this unstable system is popular among researchers around the world [1]. [2]. Consequently, it has been used by many research groups to implement self-balanced robots [3], [4]. The two-wheel mobile manipulator is one of the most recent self-balanced robots in which inverted pendulum control has been used [5]. It has the ability to balance on its two wheels and spin on the spot. This additional maneuverability allows the robot to navigate easily on various terrains, turn sharp corners, and traverse small steps or curbs.

The robot is dynamically unbalanced since there are no casters. Hence, a double-inverted pendulum controller was used for balancing our two-wheel robot since the control of a double-inverted pendulum is much easier than controlling each and every active joint. The robot consists of three manipulator links and its body, which connects manipulator part and the wheel system. Assuming that the robot's body works as a manipulator link, we have a four-link manipulator. Therefore, the manipulator system is a 4-DOF manipulator system.

When the degrees of freedom become higher, system mass is higher. The high mass of the system makes the stiffness less significant. Therefore, the relatively small stiffness of the system tends to cause unnecessary vibrations of the manipulator. The dynamic stability of this system depends on the center of gravity (COG) positions of the double-inverted pendulum. When the vibrations of manipulator links are present, the response of COG positions becomes worse. This implies that system stability deteriorates when the vibrations of manipulator links are present.

Therefore, arm vibration should be well suppressed. Several vibration-control methods have been reported [6], [7]. Meanwhile, a reaction torque observer can be used to detect external inputs without having sensor [7], [8].

The vibration suppression of a two-mass resonant system, where the resonance frequency of the motor portion is controlled by the feedback of the estimated reaction torque, has been reported [9]. This simple sensorless control strategy has been further developed by introducing displacement feedback by the elastic deformation of the arm [10] and, later, for multiple-mass systems [11].

The vibration suppression of a three-mass torsional system has been proposed by imperfect derivative feedback of the estimated torque [12]. However, there is no vibration-control methods that have been proposed for a linear mobile system which has more than two masses. A strategy of vibration suppression of a redundant manipulator by using a work-space observer and resonance ratio control based on null-space control has already been proposed [13]. A model reference zero-vibration controller has been proposed to improve the transient

Manuscript received June 15, 2008; revised December 26, 2008 and August 4, 2009; accepted January 19, 2010. Date of publication March 1, 2010; date of current version November 10, 2010.

The authors are with the Department of System Design Engineering, Keio University, Yokohama 223-8522, Japan (e-mail: kumara@sum.sd.keio.ac.jp; mura@sd.keio.ac.jp).

Color versions of one or more of the figures in this paper are available online at http://ieeexplore.ieee.org.

Digital Object Identifier 10.1109/TIE.2010.2044115

performance of robotics manipulator [14]. It is hard to find a two-wheel manipulator system where reaction torque feedback has been employed for vibration control.

The vibration control of manipulators in two-wheel mobile manipulator using resonance ratio control at null space is proposed in this paper. The application of resonance ratio control at null space of the manipulator holds our main point of originality. In addition to this, our approach holds the following original points.

1) We have applied vibration-suppression control methods to a mobile system where wheels and manipulator have dynamically interacted. No other system can be found with similar control scheme.
2) In this paper, vibration-suppression control has been implemented for a system where double-inverted pendulum control has been employed. We could not find the papers where vibration control is applied with inverted pendulum control.
3) Resonance-ratio-control-based vibration-suppression control has been implemented for multimass system with passive joint. This is another point of originality that this paper holds.

Expanding resonance ratio control for a multimass system has a long calculation process if we consider all masses separately. This complexity was eliminated by applying resonance ratio control at the null space of the manipulator. Another feature of the proposed approach is the improvement of robustness against parameter variation.

This paper is organized in eight sections as follows. This paper starts with the introduction, which explains the purpose and the background. Section II is the modeling under which dynamics and kinematics are explained. Sections III and IV are resonance ratio control and observers, respectively. Section V explains the controller design. This is the most important section, and it has two parts: posture controller with resonance ratio control and stabilization through wheel controller. Sections VI and VII are simulation and experiments. Last, this paper is wrapped up with the conclusion.

II. Modeling

The model of the two-wheel mobile manipulator (Fig. 1) is described in this section. The two-wheel robot has a coaxial two-wheel system. A direct current (dc) servomotor with an encoder used to measure wheel angle has been mounted on one wheel. A vehicle body with three-link manipulators and a wheel system are assembled together. Each manipulator link is controlled using a dc servomotor with encoder. The body is connected to the wheel system via a passive joint. The angle of the passive joint is measured using an inclination sensor. The body connected through the passive joint is also assumed to be a manipulator link.

A. Dynamics

The dynamic modeling is described in this section. The model of the robot is shown in Fig. 2. The variables of this model are given in Table I.

Fig. 1. Two-wheel mobile manipulator.

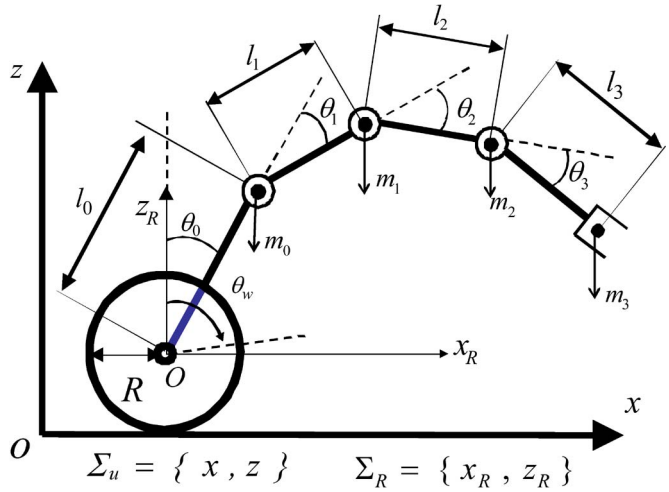

Fig. 2. Model of two-wheel mobile robot.

TABLE I
Dynamic Model Parameters

θ_i	i=w,0,1,2,3 angles of wheel, passive joint and links 1,2,3
m_i	i=w,0,1,2,3 masses of wheel, passive joint and links 1,2,3
l_0	Distance between wheel centre and centre of body
l_i	The length of the *i*th link
R	Radius of wheel
Σ_u	Universal coordinate
Σ_R	Robot coordinate

In this derivation, we have assumed that the mass of a link is located on the top of the link. θ_0 is the angle of the passive joint, and the manipulator works in x–z plane. x axis is selected horizontally parallel to the floor, and z-axis is selected vertically. x_R and z_R are the robot's coordinates. Clockwise rotation of the vehicle body, wheels, and all links are positive. In this model, dynamic equations are formulated using the Lagrange equation of motion.

The Lagrange equation is shown in

$$\frac{d}{dt}\left(\frac{\partial L}{\partial \dot{\theta}_i}\right) - \frac{\partial L}{\partial \theta_i} = \tau_i, \qquad i = 1, 2, \ldots, n. \tag{1}$$

TABLE II
PARAMETERS OF LAGRANGE EQUATION

L	Lagranrian function
T	Kinetic energy of the system
U	Potential energy of the system
τ_i	External torques

L is called the Lagrangian function and is given by "$L = T - U$." The definitions of parameters are given by Table II. The kinetic energy, potential energy, and external torques were calculated and substituted to (1), and the dynamics of the system was obtained as

$$\boldsymbol{\tau} = \boldsymbol{M}\ddot{\boldsymbol{\theta}} + \boldsymbol{H} + \boldsymbol{G} \tag{2}$$

where $\boldsymbol{\tau}$ is the vector of motor torques. $\boldsymbol{M}$ is the inertia matrix. $\boldsymbol{H}$ represents the Coriolis acceleration coefficient and centrifugal acceleration coefficient. $\boldsymbol{G}$ represents gravity.

B. Double-Inverted Pendulum

Double-inverted pendulum model is shown in Fig. 3. Here, we assumed that mass is located at the tip of the link.

In our system, we have three-link manipulators and the robot body. Therefore, the manipulator system has 4 DOF. Equivalent mass center and its positions (Table III) can be calculated for this system as (3) and (4). At this point, we have the robot body and a virtual inverted pendulum. Ultimately, it becomes a virtual double-inverted pendulum system [5]. We used abbreviations to express (3) and (4), and those are given in (5)

$$G_x = \frac{m_0 l_0 S_0 + m_1 l_1 S_{01} + m_2 l_2 S_{012} + m_3 l_3 S_{0123}}{m_0 + m_1 + m_2 + m_3} \tag{3}$$

$$G_z = \frac{m_0 l_0 C_0 + m_1 l_1 C_{01} + m_2 l_2 C_{012} + m_3 l_3 C_{0123}}{m_0 + m_1 + m_2 + m_3} \tag{4}$$

$$\left.\begin{aligned} S_0 &= \sin\theta_0 \\ C_0 &= \cos\theta_0 \\ S_{01} &= \sin(\theta_0 + \theta_1) \\ C_{01} &= \cos(\theta_0 + \theta_1) \\ S_{012} &= \sin(\theta_0 + \theta_1 + \theta_2) \\ C_{012} &= \cos(\theta_0 + \theta_1 + \theta_2) \\ S_{0123} &= \sin(\theta_0 + \theta_1 + \theta_2 + \theta_3) \\ C_{0123} &= \cos(\theta_0 + \theta_1 + \theta_2 + \theta_3) \end{aligned}\right\}. \tag{5}$$

The length and angle of the second pendulum are given by

$$l_d = \sqrt{(G_x - l_0 S_0)^2 + (G_z - l_0 C_0)^2} \tag{6}$$

$$\theta_d = \sin^{-1}\left(\frac{G_x - l_0 S_0}{l_d}\right). \tag{7}$$

A dynamic equation of the double-inverted pendulum is derived by using (1) and is given as shown in

$$\boldsymbol{\tau_d} = \boldsymbol{M}_d(\boldsymbol{q})\ddot{\boldsymbol{q}} + \boldsymbol{h}_d(\boldsymbol{q}, \dot{\boldsymbol{q}}) + \boldsymbol{g}_d(\boldsymbol{q}) \tag{8}$$

where $\boldsymbol{q} = [x, \theta_0, \theta_d]^{\mathrm{T}}$ $\boldsymbol{\tau} = [F, 0, 0]^{\mathrm{T}}$ $\boldsymbol{M}_d(\boldsymbol{q})$ is a 3×3 symmetric matrix, and components are given in Table IV. Matrices $\boldsymbol{h}_d(\boldsymbol{q}, \dot{\boldsymbol{q}})$ and $\boldsymbol{g}_d(\boldsymbol{q})$ are given by

$$\boldsymbol{h}_d = \begin{bmatrix} -(m_0 + M_1) l_0 \sin\theta_0 \dot{\theta_0}^2 - M_1 l_d \sin\theta_d \dot{\theta_d}^2 \\ M_1 l_0 l_d \sin(\theta_0 - \theta_d)\dot{\theta_0}\dot{\theta_d} \\ M_1 l_0 l_d \sin(\theta_0 - \theta_d)\dot{\theta_0}^2 \end{bmatrix} \tag{9}$$

$$\boldsymbol{g}_d = \begin{bmatrix} 0 \\ (m_0 + M_1) g l_0 \sin\theta_0 \\ M_1 g l_d \sin\theta_0 \end{bmatrix}. \tag{10}$$

Here, m_w is the mass of wheels, m_0 is the mass of the body, and M_1 is the mass of the second pendulum and is calculated as $M_1 = m_1 + m_2 + m_3$.

III. RESONANCE RATIO CONTROL

The concept of "resonance ratio" is explained in this section. The resonance ratio is determined arbitrarily by the feedback of the estimated reaction torque in case there is no error and delay in the estimated process. A two-mass resonance system is shown in Fig. 4, and it is constructed based on the assumption that there is no reduction gear in a driven system (Table V).

The estimated reaction torque is fed back to the controlled plant which is an acceleration control system of the motor portion, and it is shown in Fig. 5. K_r is the arbitrary feedback gain of reaction torque. According to Fig. 5, the transfer functions from θ_{ref} to θ_m and θ_m to θ_a are represented as shown, respectively, in

$$\frac{\theta_m}{\ddot{\theta}^{\mathrm{ref}}} = \frac{M_a s^2 + K_f}{M_a s^2 + K_f(1 + K_r M_a)} \frac{1}{s^2} \tag{11}$$

$$= \frac{s^2 + \omega_a^2}{s^2 + \omega_m^2} \frac{1}{s^2} \tag{12}$$

$$\frac{\theta_a}{\theta_m} = \frac{K_f}{M_a s^2 + K_f} \tag{13}$$

$$= \frac{\omega_a^2}{s^2 + \omega_a^2}. \tag{14}$$

ω_a is the resonance frequency of the arm portion and is acted as the counter resonant zero in the motor portion. ω_m is the resonance frequency of the motor portion, and it is controlled by the feedback of the reaction torque. K is the resonance ratio, and the definitions of ω_a, ω_m, and K are given by

$$\omega_a = \sqrt{\frac{K_f}{M_a}} \tag{15}$$

$$\omega_m = \sqrt{\frac{K_f}{M_a}(1 + K_r M_a)} \tag{16}$$

$$K = \frac{\omega_m}{\omega_a} = \sqrt{1 + K_r M_a}. \tag{17}$$

A motion controller is modified by applying proportional and derivative (PD) control to the resonance ratio system. A semiclosed loop in the motor portion is constructed for arm

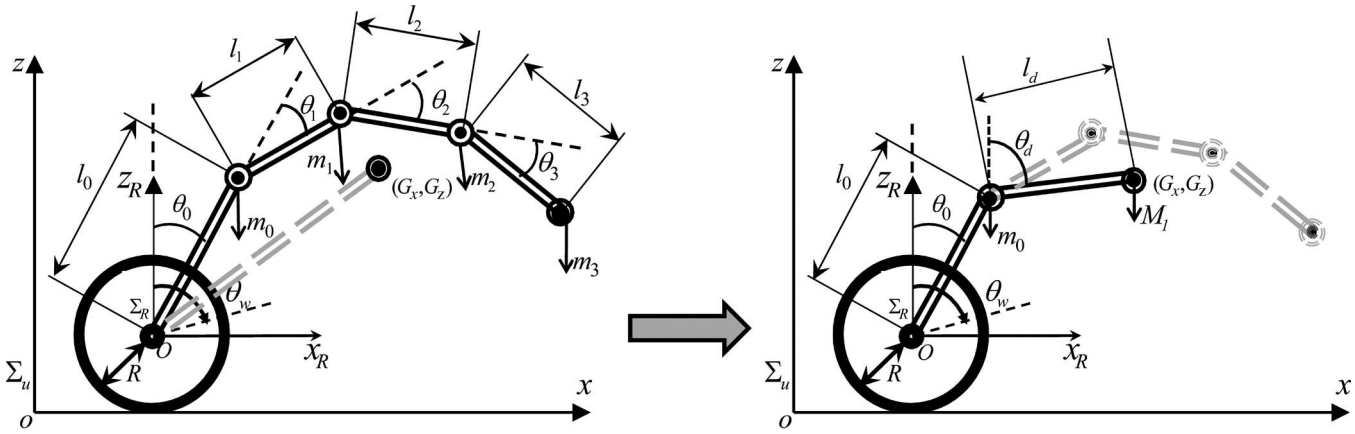

Fig. 3. Double-inverted pendulum model.

TABLE III
PARAMETERS—VIRTUAL DOUBLE-INVERTED PENDULUM

G_x	x position of COG
G_z	z position of COG
l_d	Length of second pendulum
θ_d	Angle of second pendulum

TABLE IV
ELEMENTS OF $\boldsymbol{M}_d(\boldsymbol{q})$

$m_{d11} = (m_w + m_0 + M_1)$	$m_{d12} = m_{d21} = (m_0 + M_1) l_0 cos\theta_0$
$m_{d22} = (m_0 + M_1) l_0 cos\theta_0$	$m_{d13} = m_{d31} = M_1 l_d cos\theta_d$
$m_{d33} = M_1 l_d^2$	$m_{d23} = m_{d32} = M_1 l_0 l_d cos(\theta_0 - \theta_d)$

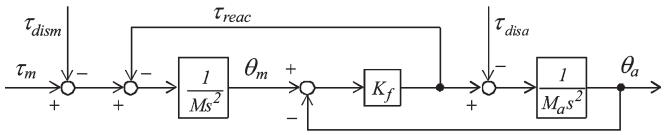

Fig. 4. Two-mass resonance system.

TABLE V
PARAMETERS—RESONANCE RATIO CONTROL

M	Motor inertia	τ_{reac}	Reaction torque
M_a	Arm inertia	τ_{disa}	Arm disturbance torque
K_f	Spring constant	τ_{dism}	Motor disturbance torque
θ_m	Motor angle	θ_a	Arm angle

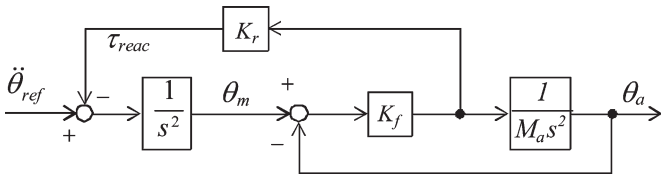

Fig. 5. Reaction torque feedback.

sensorless control. The transfer functions and the control diagram are given in the following equations and Fig. 6:

$$\frac{\theta_m^{\rm res}}{\theta^{\rm cmd}} = \frac{K_{pn}\left(s^2+\omega_a^2\right)}{\Lambda} \tag{18}$$

$$\frac{\theta_a^{\rm res}}{\theta^{\rm cmd}} = \frac{K_{pn}\omega_a^2}{\Lambda}. \tag{19}$$

$$\Lambda = s^4 + K_{vn}s^3 + (K_{pn}+\omega_m^2)s^2 + K_{vn}\omega_a^2 s + K_{pn}\omega_a^2.$$

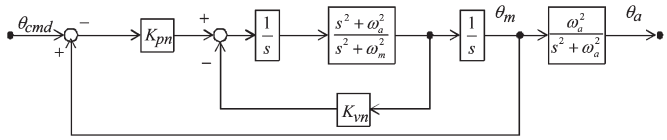

Fig. 6. PD control with resonance ratio system.

In a two-mass resonant system, a position control system is a fourth-order system in minimum realization. Therefore, it is possible to determine pole placement arbitrary when four state variables are fed back. However, the two-mass resonance system has only three parameters, and those can be selected as

$$K_r = \frac{4}{M_a} \qquad K_{pn} = \omega_a^2 \qquad K_{vn} = 4\omega_a. \tag{20}$$

IV. OBSERVERS

A. Disturbance Observer

In this paper, a disturbance observer is used to cancel the effect of disturbances to the system [17]. The total disturbance torque $\tau_{\rm dis}$ can be defined as follows:

$$\tau_{\rm dis} = \tau_{\rm int} + \tau_{\rm ext} + F + D\dot{\theta} + (M - M_n)\ddot{\theta} + (K_{tn} - K_t)I_a. \tag{21}$$

K_{tn} and M_n are the nominal torque coefficient and the inertia, respectively. $\tau_{\rm int}$ and $\tau_{\rm ext}$ are the interactive and external torques, respectively. However, disturbance torque $\tau_{\rm dis}$ can be calculated as in

$$\tau_{\rm dis} = K_{tn}I_a - M_n\ddot{\theta}. \tag{22}$$

It is hard to implement an ideal differentiator. Therefore, a pseudo differentiator is used to obtain the acceleration. Apart from this, noise is included in velocity signal. A low-pass filter is inserted to reduce the effect of this noise. The total calculation process of the disturbance can be represented as shown in (23). Fig. 7 shows the disturbance observer

$$\hat{\tau}_{\rm dis} = \frac{g_{\rm dis}}{s+g_{\rm dis}}(K_{tn}I_a + g_{\rm dis}M_n\dot{\theta}) - g_{\rm dis}M_n\dot{\theta}. \tag{23}$$

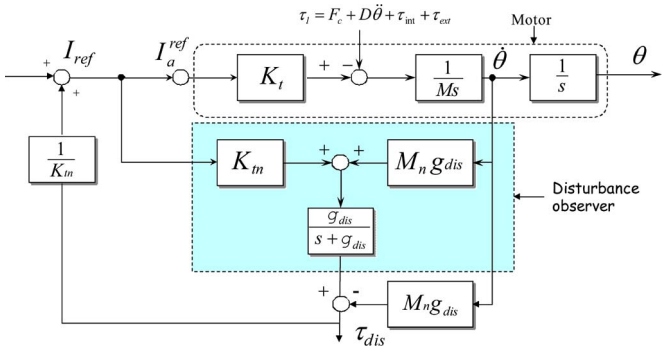

Fig. 7. Block diagram of disturbance observer.

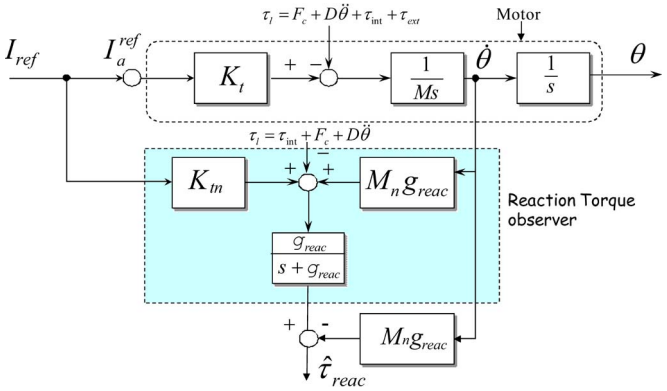

Fig. 8. Block diagram of reaction torque observer.

B. Reaction Torque Observer

The total disturbance, which is defined in (21), is used to calculate the reaction torque. It can be estimated by using the disturbance observer. Therefore, the reaction torque $\tau_{\rm reac}$ can be calculated as in

$$\tau_{\rm reac} = \tau_{\rm dis} - \tau_{\rm int} - F - D\dot{\theta} - (M - M_n)\ddot{\theta} - (K_{tn} - K_t)I_a. \tag{24}$$

Here, it is assumed that the nominal values of M_n and K_{tn} have been finely adjusted such that they are almost equal to the actual values. The total calculation process of the reaction torque observer is shown in

$$\hat{\tau}_{\rm reac} = \frac{g_{\rm reac}}{s + g_{\rm reac}}(K_{tn}I_a + g_{\rm reac}M_n\dot{\theta} - \tau_{\rm int} - F - D\dot{\theta}) - g_{\rm reac}M_n\dot{\theta}. \tag{25}$$

Fig. 8 shows the reaction torque observer.

V. Controller Design

A. Posture Controller With Resonance Ratio Control

In an n link manipulator, kinematic relationship can be expressed as shown in (26)–(28), where $\boldsymbol{q}$ is the joint angle vector, $\boldsymbol{x}$ is the position vector in work space, and $\boldsymbol{J}$ is the Jacobian matrix

$$\boldsymbol{x} = f(\boldsymbol{q}) \tag{26}$$

$$\dot{\boldsymbol{x}} = \boldsymbol{J}\dot{\boldsymbol{q}} \tag{27}$$

$$\ddot{\boldsymbol{x}} = \boldsymbol{J}\ddot{\boldsymbol{q}} + \dot{\boldsymbol{J}}\dot{\boldsymbol{q}}. \tag{28}$$

Kinematics, which is represented by $f(\boldsymbol{q})$, is the transformation of robot coordinates into world coordinates. In the redundant manipulator, the joint-space acceleration reference, which was obtained using a pseudoinverse matrix, can be written as (29). In (29), the first term is the work-space acceleration, and the second term represents the null-space motion

$$\ddot{\boldsymbol{q}}^{\rm ref} = \boldsymbol{J}^{+}(\ddot{\boldsymbol{x}}^{\rm ref} - \dot{\boldsymbol{J}}\dot{\boldsymbol{q}}) + (\boldsymbol{I} - \boldsymbol{J}^{+}\boldsymbol{J})\ddot{\boldsymbol{\phi}} \tag{29}$$

where $\boldsymbol{J}^{+}$ is the weighted pseudoinverse matrix and is defined as

$$\boldsymbol{J}^{+} = W^{-1}(\boldsymbol{J}^{\rm T}\boldsymbol{J}W^{-1}\boldsymbol{J}^{\rm T})^{-1}. \tag{30}$$

In (30), $\boldsymbol{W}$ is a diagonal weighting matrix. In the joint-space disturbance-observer-based acceleration controller, $\boldsymbol{W}$ corresponds to virtual inertia matrix $(\boldsymbol{I}_{vn})$ and can be selected arbitrarily [18]. By using the joint- and work-space observers in (29), it can be rewritten as (31) without calculating the $\dot{\boldsymbol{J}}\dot{\boldsymbol{q}}$ and $(\boldsymbol{I} - \boldsymbol{J}^{+}\boldsymbol{J})$ terms [19]

$$\ddot{\boldsymbol{q}}^{\rm ref} = \boldsymbol{J}^{+}\ddot{\boldsymbol{x}}^{\rm ref} + \ddot{\boldsymbol{q}}^{\rm ref}_{\rm null}. \tag{31}$$

Equation (32) gives the acceleration reference in work space

$$\ddot{\boldsymbol{x}}^{\rm ref} = K_{hp}(\boldsymbol{x}^{\rm cmd} - \boldsymbol{x}) + K_{hv}(\dot{\boldsymbol{x}}^{\rm cmd} - \dot{\boldsymbol{x}}) \tag{32}$$

where K_{hp} and K_{hv} are the proportional gain and derivative gain, respectively.

In this approach, $\boldsymbol{q}$ is defined by $\boldsymbol{q} = (\theta_0, \theta_1, \theta_2, \theta_3)$, and $\boldsymbol{x}$ is the $\boldsymbol{x}_{\rm cog}$ and defined by $\boldsymbol{x}_{\rm cog} = \{G_x, G_z\}$. The COG positions of the inverted pendulum are controlled at work space. Hence, (32) can be rewritten as (33). Superscipts cmd, res, and ref represent the command, response, and reference values, respectively

$$\ddot{\boldsymbol{x}}^{\rm ref}_{\rm cog} = K_{hp}\left(\boldsymbol{x}^{\rm cmd}_{\rm cog} - \boldsymbol{x}^{\rm res}_{\rm cog}\right) + K_{hv}\left(\dot{\boldsymbol{x}}^{\rm cmd}_{\rm cog} - \dot{\boldsymbol{x}}^{\rm res}_{\rm cog}\right). \tag{33}$$

In the general dynamics method, the null-space damping factor is essential for the stable convergence of the manipulator configuration. There is no damping factor that exists in null space because the virtual dynamics do not include the damper. Therefore, velocity input with damping factor was introduced in a general approach, as shown in (34). Another purpose of using velocity-based null-space input is to control null space without affecting work space [20], [21].

$$\ddot{\boldsymbol{q}}^{\rm ref}_{\rm null} = \boldsymbol{K}_{\rm null}(\dot{\boldsymbol{q}}^{\rm cmd} - \dot{\boldsymbol{q}}). \tag{34}$$

Null-space acceleration references are modified by introducing reaction torque feedback and selected as (37)

$$\ddot{\boldsymbol{q}}^{\rm ref}_{\rm null} = \left(\ddot{q}^{0}_{\rm null}, \ddot{q}^{1}_{\rm null}, \ddot{q}^{2}_{\rm null}, \ddot{q}^{3}_{\rm null}\right)^{T} \tag{35}$$

$$\ddot{q}^{0}_{\rm null} = 0.0 \tag{36}$$

$$\ddot{q}^{i}_{\rm null} = K_{pn}\left(q^{\rm cmd}_{i} - q_i\right) + K_{vn}\left(\dot{q}^{\rm cmd}_{i} - \dot{q}_i\right) - K_{ri}\tau^{i}_{\rm reac} \tag{37}$$

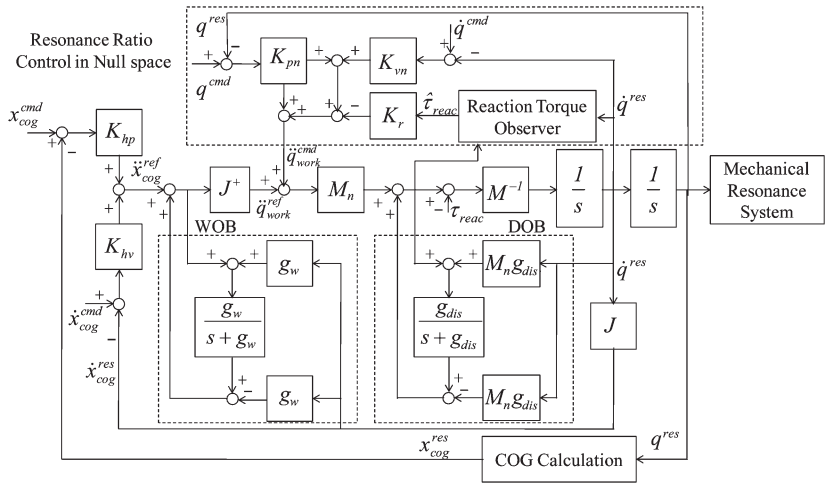

Fig. 9. Manipulator controller with vibration suppression.

where i is 1, 2, and 3. Gains K_{pn}, K_{vn}, K_{r1}, K_{r2}, and K_{r3} were selected, referring to the resonance ratio control, as given in (20). The control system with vibration control is shown in Fig. 9. In our approach, the manipulator is controlled by controlling the double-inverted pendulum, where commands are given by $\boldsymbol{x}_{\rm cog}^{\rm cmd}$ and $\dot{\boldsymbol{x}}_{\rm cog}^{\rm cmd}$. Then, we know the commands of G_x and G_z and its derivatives. In the meantime, we decide the commands of the passive joint $\theta_0^{\rm cmd}$ and $\dot{\theta}_0^{\rm cmd}$ to stabilize the passive joint angle. The design of these commands imply that the commands to the second pendulum have been virtually designed because (6) and (7) describe the calculation of θ_d. In fact, this calculation is an internal process that is done by the controller itself.

B. Stabilization Through Wheel Controller

The dynamics of the double-inverted pendulum are given in matrix form, as explained by (8)–(10). Assuming that the passive joint angle θ_0 and the angle of the second pendulum θ_d are small angles, we simplify the second row of matrix equation of (8). Since l_0 is not equal to zero, (38) was obtained. The relationship between the linear acceleration and the angular acceleration of wheels is shown as (39). Stabilization control of the two-wheeled mobile manipulator was implemented using

$$\ddot{\theta}_0 = -\frac{1}{l_0}\left(\ddot{x}_v + \frac{M_1 l_d \ddot{\theta}_d}{m_0 + M_1} + g\theta_0\right) \tag{38}$$

$$\ddot{x}_v = R\ddot{\theta}_w. \tag{39}$$

In our system, θ_0, which does not have a control input, is the angle of the passive joint. In order to stabilize the whole system, it is necessary to control θ_0. The only way that θ_0 can be controlled is to control the wheel acceleration. Hence, the following control equation is approximated:

$$\ddot{\theta}_w = K_{pd}\left(\theta_0^{\rm res} - \theta_0^{\rm cmd}\right) + K_{vd}\left(\dot{\theta}_0^{\rm res} - \dot{\theta}_0^{\rm cmd}\right) - \frac{M_1 l_d \ddot{\theta}_d}{(m_0 + M_1)R}. \tag{40}$$

K_{pd} is the position gain of the wheel command estimation, and K_{vd} is the velocity gain of the wheel command estimation. $\theta_0^{\rm res}$ and $\dot{\theta}_0^{\rm res}$ are the angle and angular velocity of robot body or passive joint, respectively, which are measured using a gyro sensor. $\theta_0^{\rm cmd}$ and $\dot{\theta}_0^{\rm cmd}$ are the command values and equal to zero. $(M_1 l_d \ddot{\theta}_d/(m_0 + M_1)R)$ is the interactive effect of the second pendulum. Equation (40) was substituted with (38) and (39) combined, and a Laplace transformation was performed for the resultant equation. Finally, $G(s)$ can be obtained

$$G(s) = \frac{\theta_0^{\rm res}}{\theta_0^{\rm cmd}} = \frac{\frac{R}{l_0}(K_{pd} + K_{vd}s)}{s^2 + \frac{R}{l_0}K_{vd}s + \frac{1}{l_0}(RK_{pd} + g)} \tag{41}$$

$$\omega_n = \sqrt{\frac{1}{l_0}(RK_{pd} + g)} \qquad \zeta = \frac{K_{vd}R}{2l_0\omega_n}. \tag{42}$$

This is a second-order transfer function. Natural angular frequency ω_n and damping coefficient ζ are given in (42). K_{pd} and K_{vd} were selected such that the system is stable. To realize the wheel control, the angular acceleration of wheel $\ddot{\theta}_w$, which was estimated as described in (40), was taken as an acceleration command to the wheel motors. Then, the estimated angular position and angular velocity are generated by integrating the angular acceleration command. The calculation process is represented by (43). Finally, the estimated angular position and angular velocity are taken as angular position command $\theta_w^{\rm cmd}$ and angular velocity command $\dot{\theta}_w^{\rm cmd}$ to the wheel motor, as described in (44)

$$\dot{\theta}_w = \int \ddot{\theta}_w\, dt \qquad \theta_w = \int \dot{\theta}_w^{\rm cmd}\, dt \tag{43}$$

$$\ddot{\theta}_w^{\rm cmd} = \ddot{\theta}_w \qquad \dot{\theta}_w^{\rm cmd} = \dot{\theta}_w \qquad \theta_w^{\rm cmd} = \theta_w. \tag{44}$$

Commands to wheel control $(\dot{\theta}_w^{\rm cmd}, \theta_w^{\rm cmd})$ were derived using an inverted pendulum model, as shown in (43). This interaction between pendulum model and wheels would guarantee the stabilization of the passive joint. These angular

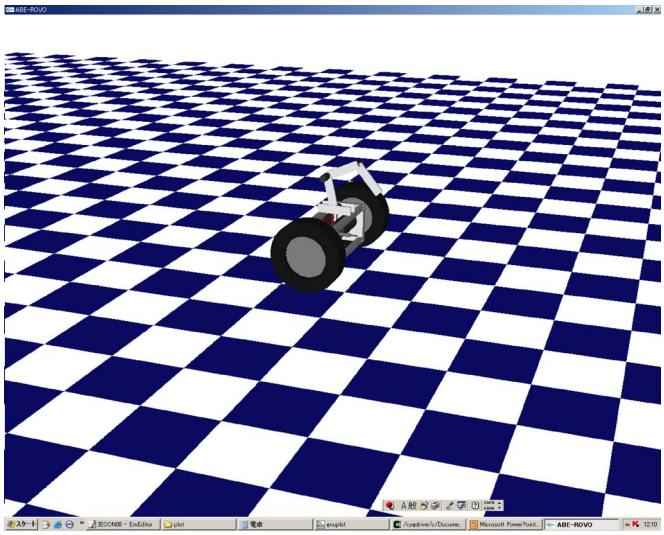

Fig. 10. Simulation setup.

TABLE VI
SIMULATION PARAMETERS

K_{pd}	80.0	K_{vd}	22.6	K_{hp}	900.0
K_{hv}	60.0	K_r	10.4	K_{pn}	225.0
K_{vn}	60.0	K_p	900.0	K_v	48.0

commands can be converted into linear commands, as shown in (45) and (46). Hence, the acceleration reference of the wheel was drawn, as described by (47). K_p and K_v are the proportional gain and velocity gain of the wheel controller, respectively

$$\dot{x}_v^{\mathrm{cmd}} = R\dot{\theta}_w^{\mathrm{cmd}} \tag{45}$$

$$x_v^{\mathrm{cmd}} = R\theta_w^{\mathrm{cmd}} \tag{46}$$

$$\ddot{x}_v^{\mathrm{ref}} = K_p\left(x_v^{\mathrm{cmd}} - x_v^{\mathrm{res}}\right) + K_v\left(\dot{x}_v^{\mathrm{cmd}} - \dot{x}_v^{\mathrm{res}}\right). \tag{47}$$

VI. SIMULATIONS

Simulation was carried out to check the validity of the proposed system, and it was implemented using OpenGL graphics software, as shown in Fig. 10. Initially, simulation was conducted without the proposed method, and data were collected. After that, simulation was repeated with the proposed method. Instead of observing position responses of each and every manipulator motor, the COG positions of the inverted pendulum were observed in this simulation. Since the proposed method has the advantage of robustness against the parameter variation, we conducted two additional tests by varying the masses and lengths of the pendulum. Simulation parameters are shown in Table VI, and results are shown in Figs. 11 and 12. In Figs. 11 and 12, line 1 shows the results with masses of $\{m_0, m_1, m_2, m_3\} = \{13.0, 1.06, 0.84, 0.5\}$ kg and lengths of $\{l_0, l_1, l_2, l_3\} = \{0.125, 0.2, 0.2, 0.18\}$ m. Line 2 shows the results with masses of $\{m_0, m_1, m_2, m_3\} = \{14.0, 1.16, 0.94, 0.6\}$ kg and the same length values. Line 3 shows the results with lengths

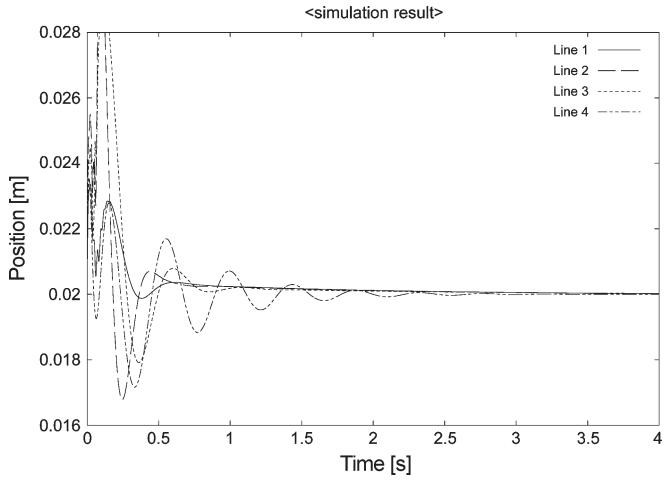

Fig. 11. Variation of the x position of COG.

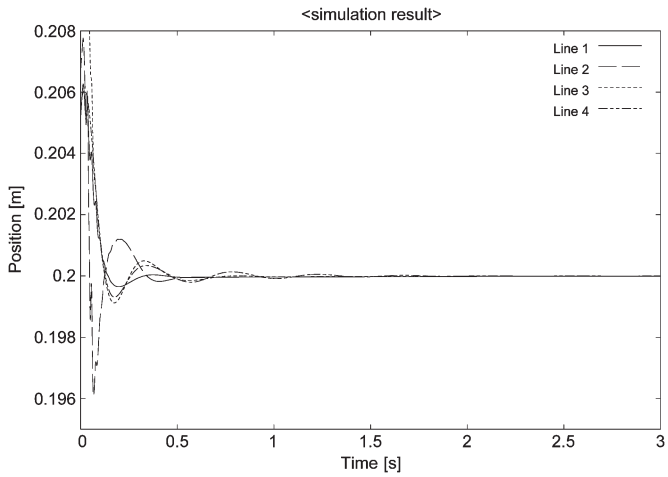

Fig. 12. Variation of the z position of COG.

of $\{l_0, l_1, l_2, l_3\} = \{0.225, 0.3, 0.3, 0.28\}$ m and the same mass values of $\{m_0, m_1, m_2, m_3\} = \{13.0, 1.06, 0.84, 0.5\}$ kg. Line 4 shows the result without the proposed resonance ratio control.

VII. EXPERIMENTS

The two-wheel mobile manipulator, which is shown in Fig. 1, was used for the experiment. Table VII explains the experimental and robot parameters that were utilized for the experiment and their values. During the experiment, the robot was set to move forward and the floor made uneven by laying down some iron plates. This was because running the robot on a rough surface creates a better picture about the effectiveness of a proposed method. First, the experiment was conducted without the proposed method, and data were collected. In this case, null-space acceleration references were generated using (37). The COG positions of the virtually modeled pendulum were observed, and results are shown in Figs. 13 and 14. In both figures, continuous lines show the commands, and the dashed lines show the results with vibration-suppression control. The remaining dotted lines are the results without the

TABLE VII
EXPERIMENT PARAMETERS

K_{pd}	10.5	K_{vd}	27.2	K_{hp}	900.0	K_{hv}	60.5
K_{pn}	246.7	K_{vn}	62.8	K_p	900.0	K_v	60.0
K_{r1}	11.5	K_{r2}	8.9	K_{r3}	6.0	-	-
$\{M_w, m_0, m_1, m_2, m_3\}$				$\{8.5, 13.0, 1.06, 0.84, 0.5\}$kg			
$\{R, l_0, l_1, l_2, l_3\}$				$\{0.2, 0.125, 0.2, 0.2, 0.18\}$m			

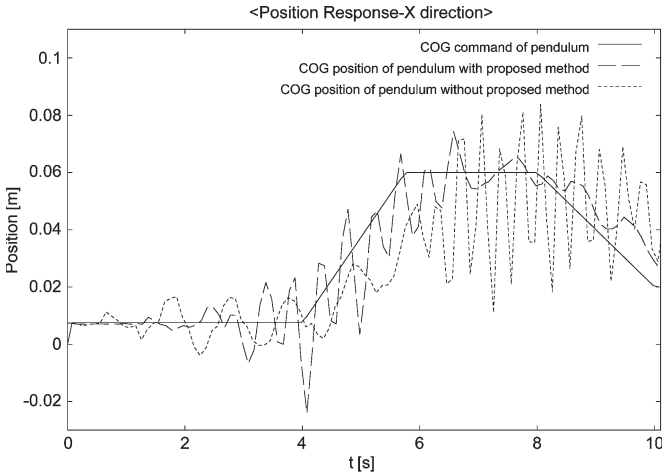

Fig. 13. COG position response in x-direction.

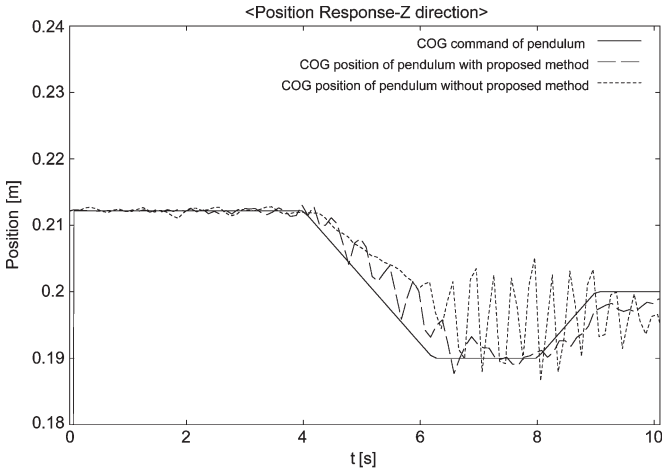

Fig. 14. COG position response in z-direction.

proposed method. Both results prove that the vibration has been reduced.

Fig. 15 shows the position response of the wheel. The total distance traveled by the robot was 3.8 m in both cases. The continuous line represents the result with the proposed method, while the dashed line gives the result without resonance ratio control. If vibrations of a system are fully suppressed, system response becomes slower. Hence, balance should be maintained between vibration control and system response. In this experiment, Fig. 15 proves that wheel response becomes faster with the resonance ratio control. The error between commands and the responses with the proposed methods has been reduced in Figs. 13 and 14. In this viewpoint, the proposed controller has reduced the vibrations while maintaining good system response.

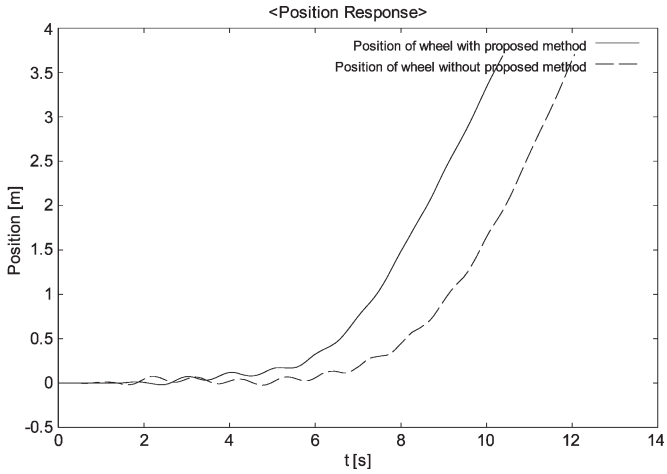

Fig. 15. Position response of wheel.

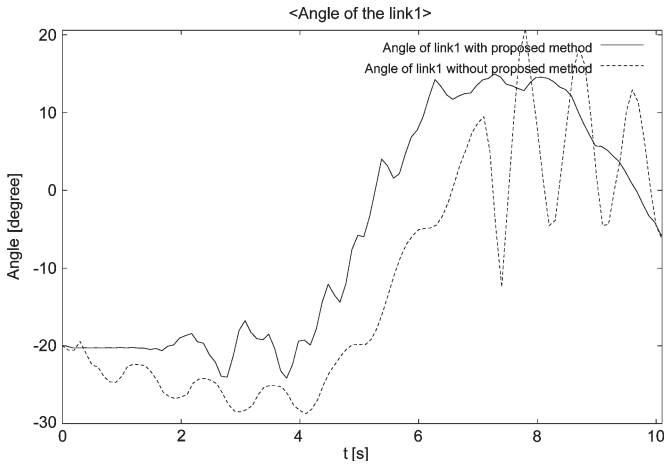

Fig. 16. Angle of link 1.

Manipulator links are moved individually to provide the commanded COG position of the pendulum. The responses of link angles were observed with and without the proposed method. In Figs. 16–18, the continuous lines represent the results with the proposed method. The dotted lines represents those cases where no resonance ratio control has been applied. It is clear that the responses of all three links have been improved, and this is due to the introduction of reaction torque feedback. The desired COG positions are achieved by moving each and every manipulator link. Therefore, links are moving while COG positions are maintaining the desired values. It can be observed from Figs. 16–18. However, the backlash of the motor assembly has affected the experiment results. If we analyze Figs. 16–18 broadly, particularly Figs. 17 and 18, the effect of backlash can clearly be seen.

VIII. CONCLUSION

The vibration suppression of manipulator arms was proposed by using resonance-ratio-based null-space control. A virtual inverted pendulum was modeled using a 4-DOF manipulator, and the control of it was used to achieve the balancing of a robot. Resonance ratio was utilized to control the arm vibrations

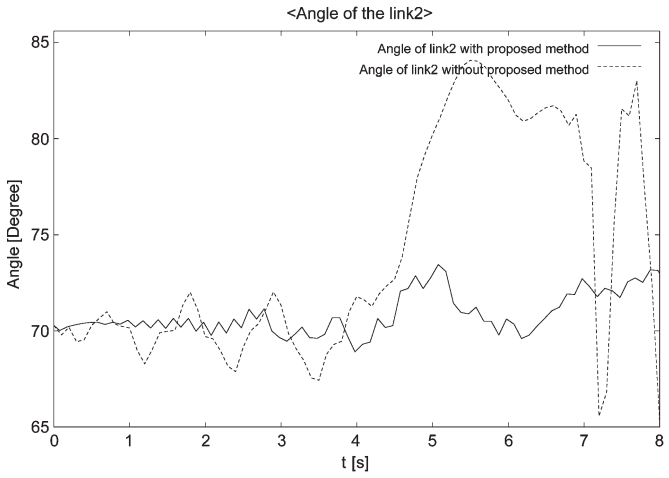

Fig. 17. Angle of link 2.

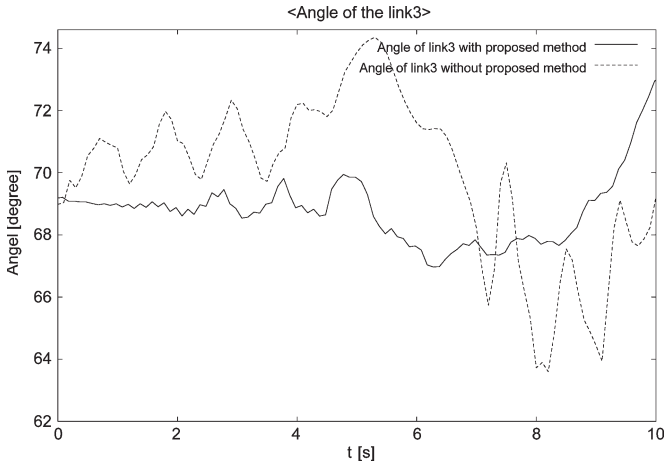

Fig. 18. Angle of link 3.

of manipulators, and it can be arbitrarily determined by using the reaction torque feedback. Reaction torque feedback was used in null space of the manipulator. The proposed method was simulated to check the validity, and simulation results verified that the proposed vibration control was effective. Introducing resonance ratio control at null space improves the robustness against parameter variation, and simulation results justify this point. The experiment was performed with the proposed method, and results showed the improvement in output of the two-wheel mobile manipulator. This method has the advantage of low-cost implementation because of the sensorless application.

In summary, this paper has developed a novel method of vibration-suppression control of a mobile system where inverted pendulum control was employed. Moreover, this paper has explained how the resonance ratio control can be used effectively with the null-space control. Experimental results proved the effectiveness of the resonance ratio control at null space. This is the most original point of this paper. In general, too much reduction of vibration in a system slows the system response. The proposed resonance-ratio-based vibration-control method has not affected the system response. Therefore, these experimental results confirm that the proposed controller is effective. The friction effect of the passive joint is high, and modeling it is not easy. This is why some gain values in experiment and simulation are different. It is not possible to model the exact friction of the passive joint in simulation. Moreover, frictions of the motors are also not exactly the same as the actual values.

REFERENCES

[1] C.-I. Huang and L.-C. Fu, "Passivity based control of the double inverted pendulum driven by a linear induction motor," in *Proc. IEEE Conf. Contr. Applicat.*, 2003, vol. 2, pp. 797–802.

[2] S. Yasunobu and T. Iwasaki, "Swing up intelligent control of double inverted pendulum based on human knowledge," in *Proc. SICE Annu. Conf.*, 2004, vol. 2, pp. 1869–1873.

[3] F. Grasser, A. D'Arrigo, and S. Colombi, "JOE: A mobile, inverted pendulum," *IEEE Trans. Ind. Electron.*, vol. 49, no. 1, pp. 107–114, Feb. 2002.

[4] I. Ko, H. Niki, and M. Toshiyuki, "Attitude control of bicycle motion by steering angle and variable COG control," in *Proc. 32nd IEEE IECON*, 2005, pp. 2065–2070.

[5] H. Abe, T. Shibata, and T. Murakami, "A realization of stable attitude control of two wheels driven mobile manipulator," in *Proc. IEEE AISM Conf.*, 2006, Paper AISM2006-A1-05, [CD-ROM].

[6] S. Kondo, K. Kaneko, and K. Ohnishi, "Vibration control of flexible joint based on link velocity estimation," in *Proc. IEEE IECON*, 1991, vol. 1, pp. 449–454.

[7] K. Yuki, T. Murakami, and K. Ohnishi, "Vibration control of flexible joint based on estimation of reaction torque," ICC-92-93, IEE Japan, 1992.

[8] Y. Ohba, M. Sazawa, K. Ohishi, T. Asai, K. Majima, Y. Yoshizawa, and K. Kageyama, "Sensorless force control for injection molding machine using reaction torque observer considering torsion phenomenon," *IEEE Trans. Ind. Electron.*, vol. 56, no. 8, pp. 2956–2960, Aug. 2009.

[9] K. Yuki, T. Murakami, and K. Ohnishi, "Vibration control of 2 mass resonant system by resonance ratio control," in *Proc. IECON*, 1993, vol. 3, pp. 2009–2014.

[10] M. Kino, T. Goden, T. Murakami, and K. Ohnishi, "Reaction torque feedback based vibration control in multi-degrees of freedom motion system," in *Proc. 24th IEEE IECON*, 1998, vol. 3, pp. 1807–1811.

[11] S. Nomura, T. Murakami, and K. Ohnishi, "Vibration control of multiple mass system by estimated reaction torque," in *Proc. 21st IEEE Int. Conf. Ind. Electron., Control, Instrum.*, 1995, vol. 2, pp. 1091–1095.

[12] K. Sugiura and Y. Hori, "Vibration suppression in 2- and 3-mass system based on the feedback of imperfect derivative of the estimated torsional torque," *IEEE Trans. Ind. Electron.*, vol. 43, no. 1, pp. 56–64, Feb. 1996.

[13] K. Sasaki and T. Murakami, "Suppression control of redundant manipulator with flexible structure by considering null space motion," *IEEE Trans. Ind. Appl.*, vol. 127, no. 10, pp. 1043–1049, 2007.

[14] D. Yuan and T. Chang, "Model reference input shaper design with applications to a high-speed robotic workcell with variable loads," *IEEE Trans. Ind. Electron.*, vol. 55, no. 2, pp. 842–851, Feb. 2008.

[15] S. Katsura and K. Ohnishi, "Force servoing by flexible manipulator based on resonance ratio control," *IEEE Trans. Ind. Electron.*, vol. 54, no. 1, pp. 539–547, Feb. 2007.

[16] S. Katsura, J. Suzuki, and K. Ohnishi, "Pushing operation by flexible manipulator taking environmental information into account," *IEEE Trans. Ind. Electron.*, vol. 53, no. 5, pp. 1688–1697, Oct. 2006.

[17] K. Ohnishi, M. Toshiyuki, and M. Shibata, "Motion control for advanced mechatronics," *IEEE/ASME Trans. Mechatronics*, vol. 1, no. 1, pp. 56–67, Mar. 1996.

[18] N. Oda, T. Murakami, and K. Ohnishi, "A force based motion control strategy for hyper-redundant manipulator," in *Proc. 23rd IECON*, 1997, vol. 3, pp. 1385–1390.

[19] T. Murakami, K. Kahlen, and R. W. A. A. De Doncker, "Robust motion control based on projection plane in redundant manipulator," *IEEE Trans. Ind. Electron.*, vol. 49, no. 1, pp. 248–255, Feb. 2002.

[20] F. Inoue, T. Murakami, and K. Ohnishi, "A motion control of mobile manipulator with external force," in *Proc. 6th Int. Workshop Adv. Motion Control*, 2000, pp. 98–103.

[21] N. Oda, T. Murakami, and K. Ohnishi, "Robust motion control in redundant motion systems," in *Proc. 5th AMC*, 1998, pp. 135–140.

Pradeep K. W. Abeygunawardhana received the B.Sc.(Eng.) degree in electrical engineering from the University of Moratuwa, Moratuwa, Sri Lanka, in 2002 and the M.E. degree from Keio University, Yokohama, Japan, in 2006, where he is currently working toward the Ph.D. degree.

His research interests are motion control of two-wheel mobile manipulator, nonlinear control, wheelchair robot, and underactuated mechanical system.

Toshiyuki Murakami (M'93) received the B.E., M.E., and Ph.D. degrees in electrical engineering from Keio University, Yokohama, Japan, in 1988, 1990, and 1993, respectively.

In 1993, he joined the Department of Electrical Engineering, Keio University, where he is currently a Professor in the Department of System Design Engineering. From 1999 to 2000, he was a Visiting Researcher with the Institute for Power Electronics and Electrical Drives, Aachen University of Technology, Aechen, Germany. His research interests include robotics, intelligent vehicles, mobile robots, and motion control.